European Radiology (2019) 29:2878–2889
https://doi.org/10.1007/s00330-018-5850-z

COMPUTED TOMOGRAPHY

Can virtual monochromatic images from dual-energy CT replace low-kVp images for abdominal contrast-enhanced CT in small- and medium-sized patients?

Peijie Lv[1] · Zhigang Zhou[1] · Jie Liu[1] · Yaru Chai[1] · Huiping Zhao[1] · Hua Guo[1] · Daniele Marin[2] · Jianbo Gao[1]

Received: 28 March 2018 / Revised: 29 September 2018 / Accepted: 22 October 2018 / Published online: 30 November 2018

Abstract

Objective To investigate the image quality and radiation dose of dual-energy computed tomography (DECT) with automatic spectral imaging protocol selection (ASIS) compared with those of low-kVp CT in abdominal multiphase CT.

Methods Four groups of 60 patients each underwent abdominal scans with low-kVp CT (A, 80 kVp/300 mg I/kg, body mass index [BMI] ≤ 23.9 kg/m^2; C, 100 kVp/400 mg I/kg, BMI ranging from 24 to 28.9 kg/m^2) or DECT with ASIS, and the 40- to 60-keV virtual monochromatic images (VMIs) generated (B and D) were matched by age, gender, BMI, cross-sectional area, and contrast agent dose; 9 patients were excluded due to technical failures. The CT number, image noise, contrast-to-noise ratio, and subjective image quality were compared between the matched protocols (A and B or C and D) on 1.25-mm reconstructed images.

Results VMIs at approximately 55 keV and 62 keV had CT numbers and contrast similar to those of 80-kVp and 100-kVp CT images, respectively. Compared to matched low-kVp images, VMIs at 50 keV provided a higher CT number and image noise and a similar or higher contrast and overall image quality. The radiation dose for DECT was higher than that of 80-kVp CT (increased by 10%), but was similar to that of 100-kVp CT.

Conclusion Compared to matched low-kVp CT, VMIs at 50 keV in DECT with ASIS provided similar or higher overall image quality, with no or minimal dose penalty in small- and medium-sized patients.

Key Points

- *Virtual monochromatic images at approximately 55 keV and 62 keV have CT numbers and contrast similar to those of 80-kVp and 100-kVp CT images, respectively, with a given noise index.*
- *The radiation dose in dual-energy CT with automatic spectral imaging protocol selection was slightly higher than that of 80-kVp CT (increased by 10%) but was similar to that of 100-kVp CT.*
- *Dual-energy CT may be able to replace l00-kVp CT for routine clinical abdominal contrast-enhanced CT scans.*

Keywords CT protocol · Tomography, X-ray computed · Image processing, computer-assisted · Radiation dosage · Cross-sectional studies

Abbreviations

AP	Arterial phase
ASIR	Adaptive statistical iterative reconstruction
ASIS	Automatic spectral imaging protocol selection
CNR	Contrast-to-noise ratio
CTDIvol	Volume computed tomography dose index
IC	Iodine concentration
keV	Kiloelectron volt
kVp	Peak kilovoltage
PVP	Portal venous phase
VMI	Virtual monochromatic images

✉ Jianbo Gao
jianbogao0307@163.com

[1] The Department of Radiology, The First Affiliated Hospital of Zhengzhou University, No.1, Eastern Jianshe Road, Zhengzhou 450052, Henan Province, China

[2] The Department of Radiology, Duke University Medical Center, Erwin Rd, Box 3808, Durham, NC 27710, USA

Introduction

Conventional computed tomography (CT) images are acquired using a polychromatic X-ray beam with a peak energy

of 80–140 kVp [1, 2] from a single-energy CT (SECT) examination. The low tube voltage CT technique (80 kVp or 100 kVp) used in abdominal CT improves the contrast enhancement of vessels and organs and reduces the radiation dose [3–5]. Similarly, virtual monochromatic images (VMI) generated from dual-energy CT (DECT) system provides higher contrast and more noise at low energy levels (40 to 60 keV) [6]. Low-energy images can be acquired with automated tube current modulation (ATCM) and noise reduction [2, 7–10].

Material decomposition (MD) images from DECT enable the measurements of iodine concentrations (ICs) for detection and characterization of different tissues [11, 12], thus expanding the diagnostic information of conventional SECT images. Automatic spectral imaging protocol selection (ASIS) technique (Gemstone Spectral Imaging (GSI) Assist, GE Healthcare) in DECT provides practical recommendations regarding the optimal spectral imaging preset based on the patient's size and preferred scan parameters. This protocol recommendation has the potential to optimize the radiation dose and the image quality of VMIs by adjusting the image acquisition parameters (rotation time, scan field of view, detector coverage, and tube current) [13]. The value of ASIS in abdominal DECT, compared to low-kVp CT, has not yet been demonstrated in small- and medium-sized patients. Previous studies [14, 15] comparing the image quality and radiation dose of DECT and SECT have mainly focused on comparisons with SECT using 120-kVp CT instead of low-kVp CT [15]. Although Yu et al [16] demonstrated the relationship between optimized VMIs in dual-source DECT and polychromatic images in low-kVp CT in a phantom study, it remains unclear whether DECT can replace low-kVp SECT for routine clinical use.

The aim of this study was to compare the image quality, radiation dose, and lesion detectability of DECT using ASIS technique with those of single-energy low-kVp CT (80 kVp and 100 kVp) for abdominal applications in matched patient cohorts.

Methods

This study was approved by our institutional review board, and written informed consent was obtained from all patients. In total, 378 consecutive patients with known or suspected primary or secondary liver lesions, chronic hepatitis, or cirrhosis based on prior treatment history, imaging findings, or a high level of tumor marker underwent multiphase liver CT. The exclusion criteria for CT were a history of hypersensitivity to iodinated contrast media, compromised renal function (estimated glomerular filtration rate < 30 mL/min/1.73 m^2), or severe cardiac insufficiency.

Two hundred forty patients were selected and divided into low-kVp group ($n = 120$) or DECT group ($n = 120$) based on the study period and imaging protocol used and were matched by age, gender, body mass index (BMI), and cross-sectional area of the abdomen (Table 1). Deviations of ± 2 years, ± 2 kg/m^2 and ± 2 cm were considered acceptable for age, BMI, and cross-sectional transverse abdomen area matching [17, 18]. In the first half of the study period, patients underwent SECT using 80 kVp (protocol A, $n = 60$) if their BMI was ≤ 23.9 kg/m^2 (underweight and normal BMI) or using 100 kVp (protocol C, $n = 60$) if their BMI ranged from 24 to 28.9 kg/m^2 (overweight) [19]. In the second half of the study period, another 120 patients underwent DECT and were matched accordingly to patients with low-kVp protocols ($n = 60$ each, protocol B vs. protocol A; protocol D vs. protocol C). If more than one subject who received protocol B (or D) had the same gender, age, and BMI as those of a patient in protocol A (or C), the patient with the most similar cross-sectional abdominal area was chosen.

Detailed information regarding the study design is summarized in Fig. 1.

CT examinations and contrast agent infusion protocols

Unenhanced and two-phase contrast material-enhanced CT examinations of the entire liver were performed for all patients using a Discovery CT750HD scanner (GE Healthcare). Unenhanced examinations were performed with the helical imaging mode at a tube voltage of 120 kVp and ATCM. The detailed contrast-enhanced CT scanning parameters of each protocol are shown in Table 1. The optimal spectral imaging presets for each patient in protocols B and D were automatically selected using ASIS. Nonionic contrast material (Iohexol, Omnipaque, 350 mg I/mL; GE Healthcare) was injected via antecubital venous access at an adjusted rate and total iodine dose based on patient body weight [20], followed by an injection of 20 mL of saline. The acquisition times for arterial-phase (AP) and portal venous-phase (PVP) images were constant at 30 s and 60 s, respectively, after contrast agent administration [13].

Based on a previous study [21], images obtained using protocols A and C were reconstructed with 50% adaptive statistical iterative reconstruction (ASIR) and a standard kernel to achieve a balance between image noise and contrast. For protocols B and D, VMIs with energy values ranging from 40 to 60 keV in 10-keV increments were reconstructed with 50% ASIR blending based on the manufacturer's recommendations and on the results of previous studies [13, 22]. Water- and iodine-based MD images were reconstructed from the spectral CT acquisition for analysis. VMIs from 40 to 70 keV in 1-keV increments were reconstructed to match the CT numbers of low-kVp images.

Table 1 Summary of demographic data of patients and scanning parameters for each protocol

	Low-kVp protocol		Spectral imaging protocol	
	Protocol A	Protocol C	Protocol B	Protocol D
Patient parameters				
Age (years)	57.1 ± 15.3	55.2 ± 15.7	57.3 ± 12.1	55.3 ± 11.2
Sex (M/F)	32/28	35/25	2/28	35/25
Weight (kg)	58.5 ± 7.4	70.2 ± 7.6	57.7 ± 8.4	72.4 ± 6.3
BMI (kg/m^2)	21.2 ± 2.5	26.3 ± 1.8	21.5 ± 2.4	26.7 ± 1.5
Abdomen AP diameter (cm)	23.6 ± 3.6	22.3 ± 2.0	23.9 ± 2.8	23.0 ± 2.6
Liver disease*				
Absent	19 (27.1)	13 (20.3)	15 (24.2)	10 (14.7)
Viral††	3 (4.3)	2 (3.1)	6 (9.7)	3 (4.4)
Liver cirrhosis	12 (17.1)	8 (12.5)	5 (8.1)	18 (26.4)
Hemangioma	6 (8.6)	7 (10.9)	4 (6.5)	9 (13.2)
Hepatocellular carcinoma	15 (21.4)	22 (34.3)	18 (29.0)	19 (27.9)
Metastasis	6 (8.6)	2 (3.1)	1 (1.6)	3 (4.4)
Other	9 (12.9)	10 (15.6)	13 (21.0)	6 (8.8)
Scanning parameters				
Tube voltage (kVp)	80	100	80 and 140	80 and 140
Tube current (mA) eff.	220–600	280–600	260–600	260–600
Gantry rotation time (s)	0.8	0.8	0.7–0.8	0.7–0.8
Detector coverage (mm)	40	40	40	40
Pitch	1.375:1	1.375:1	1.375:1	1.375:1
Scan field of view (cm)	36	50	36	50
Noise index (HU)†	10	10	10	10
Section/reconstructed thickness (mm)	5.0/1.25	5.0/1.25	5.0/1.25	5.0/1.25
Reconstruction algorithm	50% ASIR	50% ASIR	50% ASIR	50% ASIR
Reconstruction kernel	Standard	Standard	Standard	Standard
MD parameter	–	–	Iodine to water	Iodine to water
Iodine concentration (mg I/kg)	300	400	300	400

For the patient parameters, data are shown as the means and standard deviations, except for the sex ratio. No significant differences were found between protocol A and protocol B or between protocol C and protocol D in the distribution of liver diseases ($p > 0.05$)

ASIR adaptive statistical iterative reconstruction, *MD* material decomposition

*Data are shown as the frequencies of scores, with percentages in parentheses

† 5-mm section thickness

†† Hepatitis B virus or hepatitis C virus

Image analysis

Quantitative analysis

All images were transferred to a commercially available workstation (Advantage Workstation 4.6; GE Healthcare) for analyses and were reviewed using the GSI viewer. A single radiologist (P.J.L. with 7 years of clinical experience) independently and blindly measured the image noise, IC (in units of 100 μg/mL), and Hounsfield units (HU) of attenuation of the liver, abdominal aorta, portal vein, and paraspinal muscle, as described in previous reports [2, 23, 24] (Fig. 2a and b). The contrast-to-noise ratio (CNR) was calculated for the organ of interest (liver, aorta, or portal vein) as follows: CNRo = (CTo − CTm) SDn, where CTo is the mean CT number of the organ of interest, CTm is the mean CT number of the paraspinal muscle, and SDn is the mean image noise. The change in CT number or IC (ΔValue) between 300 and 400 mg I/kg for all images in organs of interest (liver, aorta, and portal vein) was calculated as follows: $\Delta Value = (Value_{400} - Value_{300})\ \ Value_{400} \times 100\%$, where Value is the CT number or IC of the organ of interest.

Qualitative analysis

Two abdominal radiologists (Z.G.Z. [observer 1] and J.B.G. [observer 2] with over 30 years of clinical experience) and one

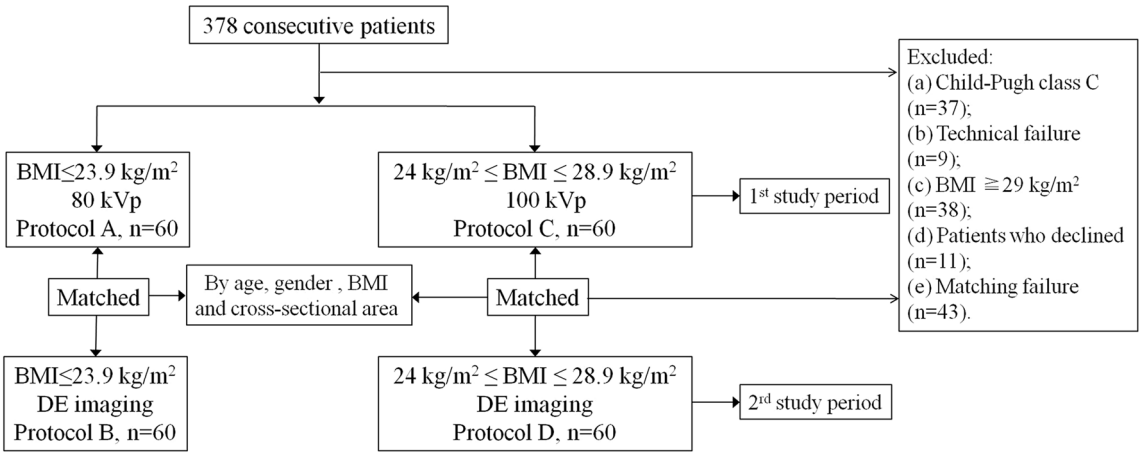

Fig. 1 Flowchart showing the patient selection and study design. Nine patients exhibited technical failure due to residual intestinal barium ($n = 6$) and three-way tube fall-off ($n = 3$). DE, dual-energy

radiologist (Y.R.C. [observer 3]) independently analyzed a total of 960 ($3 \times 120 \times 2 + 120 \times 2$) liver CT images at the level of the hepatic portal vein, including all low-kVp CT images and VMIs in the range of 40–60 keV, using the same workstation. All images were examined using a preset window setting (width, 400 HU; level, 40 HU), without including patient demographics or CT parameters, and were randomized to each reader for blind evaluation. Readers were allowed to modify the window width and level at their own discretion.

Image noise and overall image quality were assessed using 5-point subjective scales on both AP and PVP images (1, unacceptable, severe image noise and artefacts; 2, minimally acceptable, obvious image noise and artefacts, decreased anatomical structure and confidence in details; 3, acceptable image noise and artefacts, decreased confidence in details but relatively clear anatomical structure; 4, less than average image noise and artefacts, less clear anatomical structure and details; and 5, minimal image noise and artefacts, sharp anatomical structure and satisfactory details) [25], while the visibility of small vascular structures was evaluated on AP images based on a 5-point scale [13] (1, unacceptable; 2, suboptimal; 3, acceptable; 4, above average; and 5, excellent). Additionally, abdominal organ enhancement was assessed on PVP images with a three-point scoring scheme (1, unacceptable; 2, acceptable; and 3, excellent) [26].

Lesion analysis

Reference standard

Sixty-five of the total 240 patients with 74 proven hypervascular hepatocellular carcinoma (HCC) nodules ($n =$ 15, 18, 22, and 19 in protocols A, B, C, and D, respectively) were included for lesion analysis. Thirty-four HCCs in 31 patients were confirmed pathologically after percutaneous biopsy or surgery. The diagnosis of the remaining 40 HCCs in 34 patients was established by typical imaging findings and high levels of serum α-fetoprotein (> 11 ng/mL) (16 HCCs in 12 patients) or by follow-up CT examinations for lipiodized oil after transcatheter arterial chemoembolization (24 HCCs in 22 patients) performed more than 4 weeks after the procedure. Typical findings of HCC included contrast uptake in the AP and washout in the PVP [24]. In cases with more than three tumors, only the three largest tumors were included.

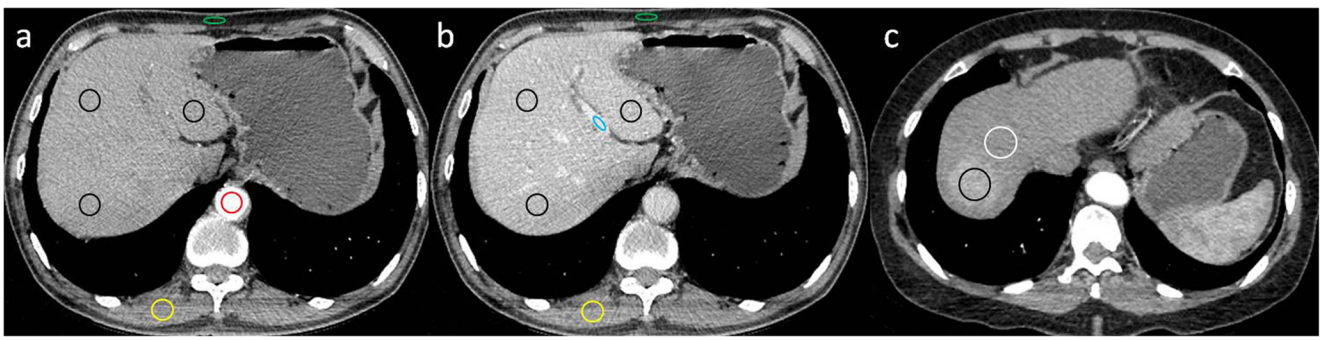

Fig. 2 Axial contrast-enhanced abdominal CT images at 80 kVp obtained in a 56-year-old man during the arterial phase (**a**) and portal venous phase (**b**), with ROIs drawn on the liver (black), aorta (red), portal vein (blue), paraspinal muscle (yellow), and subcutaneous fat of the anterior abdominal wall (green). An arterial-phase CT image at 80 kVp (**c**) in a 48-year-old woman shows placement of a region of high-enhancing area on the tumor (black) and adjacent non-tumorous liver parenchyma (white)

Tumor analysis

The tumor-to-normal parenchyma ratio (TNR) for attenuation and IC was calculated as the attenuation ratio between the high-enhancing portion of the tumor and adjacent non-tumorous liver parenchyma [6] (Fig. 2c). Tumor ICs were measured on the iodine-based MD images. The lesion numbers were recorded, and lesion conspicuity was assessed on AP images based on a 5-point scale (1, definitely an artefact mimicking a lesion; 2, likely an artefact mimicking a lesion; 3, subtle lesion; 4, fairly distinct with poorly visualized margins; 5, definitely distinct with visualized margins) [1].

Radiation dose

Considering the radiation dose for the PVP scan was acquired using the same scanning parameters, including scan length, as those used for the AP scan during a single breath-hold, the volume computed tomography dose index (CTDIvol, mGy) and dose-length product (DLP, mGy cm) values were only recorded on AP images. The estimated effective radiation dose (mSv) was obtained by multiplying the DLP with a conversion factor of 0.015 for abdominal examination [27].

Statistical analyses

All statistical analyses were performed using SAS (version 9.1.3; SAS Institute), with $p < 0.05$ indicating a statistically significant difference. An independent samples *t* test was used to compare the CT attenuation, CNR, image noise, ΔValue, tumor-to-liver ratio, and radiation dose between the matched protocols (A and B or C and D) and to compare the CT number or IC between protocols with same scanning methods (A and C or B and D). Percentage changes in CT number from 40 to 60 keV and IC for the organs of interest using the same protocol (B or D) were evaluated using one-way ANOVA, with Bonferroni's multiple comparison post hoc test for further comparisons in cases of statistical significance. The Mann-Whitney *U* test was used to analyse differences in categorical variables and qualitative parameters between the matched protocols. Inter-reader agreement for qualitative parameters was evaluated using kappa analysis with κ statistics.

Results

Quantitative analysis

VMIs from 40 to 70 keV for the organs of interest, with CT numbers equal to those of 80-kVp and 100-kVp images, were in the range of 54–56 keV (mean 55 keV, *p* values ranging from < 0.083 to 0.098) and 61–63 keV (mean 62 keV, *p* values ranging from < 0.088 to 0.096), respectively, except for the liver in the AP (both *p* values < 0.001) (Fig. 3). No significant differences were observed in the CNR between low-kVp images and VMIs at the matched energy level, despite the higher image noise (17.1 ± 6.9 HU) in VMIs at 55 keV than in 80-kVp images ($p < 0.001$).

Compared to protocol A, the mean CT numbers of VMIs in protocol B, from 40 to 60 keV, for the liver, abdominal aorta, and portal vein were significantly higher at the energy levels of 40 keV and 50 keV (all *p* values < 0.05), except for the lower value in the liver in the AP ($p < 0.001$ for each comparison), and were lower at 60 keV ($p < 0.001$ for each comparison). Compared to protocol C, the mean CT numbers of VMIs in protocol D, from 40 to 60 keV, for the organs of interest were significantly higher for the energy levels of 40 keV and 50 keV (all *p* values < 0.05), except for the liver at 40 keV ($p = 0.787$) and 50 keV ($p = 0.023$) in the AP, and they were similar or higher at 60 keV, except for the lower liver in the AP ($p < 0.001$) (Table 2).

The mean image noise for protocol A (or C) was significantly lower than that for the corresponding protocol B (or D) at 40 keV and 50 keV ($p < 0.05$ for each comparison) and was similar to that at 60 keV. Compared to the corresponding protocol A (or C), the CNR values for the liver in the range of 40–60 keV for VMIs in protocol B (or D) were all lower during the AP (all *p* values < 0.05) but were similar or higher during the PVP. The CNR values for the abdominal aorta and portal vein in the range of 40–60 keV for VMIs in protocol B (or D) were similar to or higher than those in the corresponding protocol A (or C) (A vs. B, portal vein at 40 keV, $p < 0.001$; C vs. D, portal vein at 40 keV and 50 keV, $p < 0.001$ and 0.012, respectively).

The liver, abdominal aorta, and portal vein showed no significant differences between protocols A and C for the mean CT numbers, except for the liver during the AP ($p = 0.001$). The mean CT numbers for VMIs in the range of 40–60 keV and the ICs of the organs in protocol D were all significantly higher than those in protocol B, except for the liver in the AP at 50-keV ($p = 0.073$) and 60-keV VMIs ($p = 0.189$) (Fig. 4). The ΔValues for the organs of interest in VMIs from 40 to 60 keV and the iodine-based images were all higher than those in the low-kVp images (all *p* values < 0.05), with no significant differences between VMIs and iodine-based images for all organs, except for the liver during the AP.

Qualitative analysis

The subjective image quality scores of all protocols were greater than 2, which indicated an acceptable overall image quality. Compared to low-kVp images in protocols A and C, 40-keV VMIs in the corresponding protocols B and D showed greater small vascular structure visibility ($p < 0.001$) and

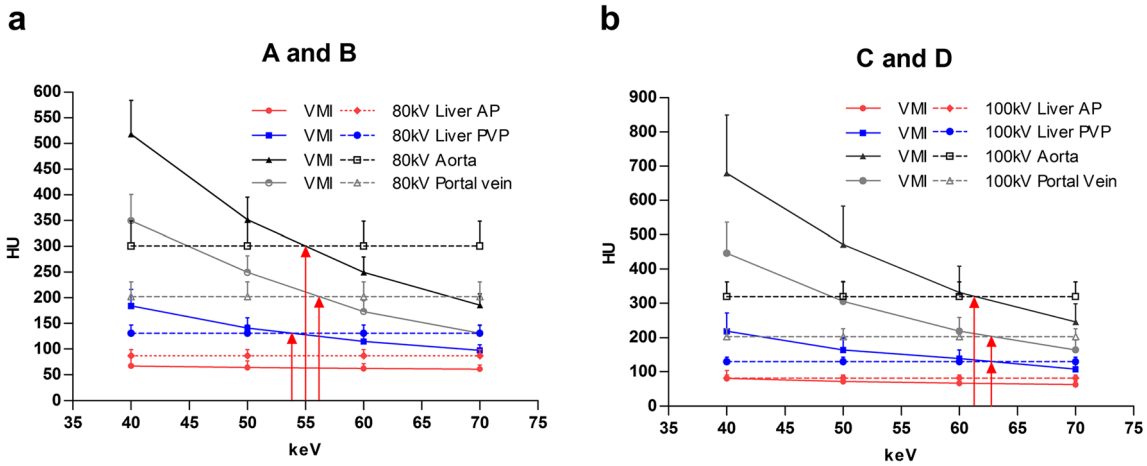

Fig. 3 Mean CT values for the liver, aorta, and portal vein on 80-kVp CT images (protocol A), 100-kVp CT images (protocol C), and monochromatic images (40 to 70 keV) in protocols B and D. The mean energy levels of the DECT protocol with CT numbers equal to those of the 80-kVp and 100-kVp protocols were approximately 55 keV in protocol B (**a**) and 62 keV in protocol D (**b**), respectively, except for the liver during the AP

abdominal organ enhancement scores ($p < 0.05$) and lower image noise scores ($p < 0.05$) but similar overall image quality in protocol B and lower overall image quality in protocol D. The analyses of the subjective readers' rankings for protocols B and D were similar or significantly higher for 50-keV and 60-keV VMIs with regard to small vascular structure visibility, image noise, abdominal organ enhancement, and overall image quality compared to the corresponding protocols A and C, except for the reduced small vascular structure visibility in 60-keV VMIs in protocol B (Table 3, Fig. 5).

Lesion analysis

Compared to protocol A (or C), the TNR and lesion conspicuity in the corresponding protocol B (or D) were significantly higher in 40-keV VMIs and in iodine-based MD images ($p < 0.05$ for each comparison) but were similar for 50-keV VMIs, except for the higher TNR at 50 keV in protocol D. VMIs at 60 keV in protocol B (or D) showed similar TNR but lower lesion conspicuity compared to those in the corresponding protocol A (or C). No significant differences were found in lesion detection rates in either matched protocol (Table 4).

Radiation dose

The CTDIvol, DLP, and effective radiation dose (10.60 ± 3.71 mGy, 262.66 ± 74.55 mGy cm, 3.93 ± 0.06 mSv) were higher in protocol B (increased by 10%) than in protocol A (8.14 ± 0.31 mGy, 237.47 ± 30.53 mGy cm, 3.56 ± 0.05 mSv) in the AP ($p = 0.001$, 0.042, and 0.042, respectively). Approximately the same distribution of CTDIvol in protocols C and D resulted in a similar radiation dose in the AP (CTDIvol, 14.39 ± 1.43 vs. 13.40 ± 3.55 mGy, $p = 0.062$; DLP, 444.06 ± 85.40 vs. 444.13 ± 99.23 mGy cm, $p = 0.998$; effective radiation dose, 6.65 ± 0.10 vs. 6.66 ± 0.10 mSv, $p = 0.998$) (Table 5). Our CTDIvols were lower than the national diagnostic reference level (25 mGy) and were similar to or lower than the values used in some European countries (14–18 mGy) [28–31].

Discussion

Our study demonstrated that CT numbers for the liver, aorta, and portal vein during the AP and PVP in VMIs at approximately 55 keV and 62 keV were similar to those on 80-kVp and 100-kVp CT images respectively, except for the liver in AP, with a given noise index. Our results are in contrast with the findings reported by Agrawal MD et al [32], who showed that approximately 60–77-keV VMIs had applications similar to those of low (80–100 kVp) DE images. However, the results of the latter study were not obtained from human studies and were also partially contradicted by the results of Matsumoto et al [33], who showed that CT numbers in VMIs at approximately 70 keV were equal to those of 120-kVp CT images and increased as the X-ray energy level decreased in vitro.

The relationship between VMIs and low-kVp CT images might explain why the image noise of VMIs at 40 keV and 50 keV in our study was higher than that of low-kVp CT images with the same ASIR percentage, which can compensate for the increased image noise at all low energy levels [8, 13, 22]. The high image noise of VMIs might be partially compensated for by an increase in the CT numbers, favoring similar or higher CNR at all low energy levels compared to low-kVp CT images, particularly at 50 keV and 60 keV, which manifested similar or higher overall image quality in our study. However, the nearly doubling in noise at 40-keV images compared to low-kVp images can offset the advantages of higher CT contrast, resulting in an overall lower image

Table 2 Quantitative analysis results in low-kVp protocols (protocols A and C) and spectral imaging protocols (protocols B and D)

Parameter	Protocol A	Protocol B				Protocol C	Protocol D			
		40 keV	50 keV	60 keV	ID		40 keV	50 keV	60 keV	ID
CT numbers (HU)					IC (100 μg/cm^3)					IC (100 μg/cm^3)
Liver during AP	87.3 ± 11.2	67.3 ± 18.8**	64.2 ± 12.7**	62.2 ± 9.3**	2.1 ± 1.6	81.0 ± 9.5	80.3 ± 22.9	71.4 ± 15.9*	66.0 ± 11.5**	3.4 ± 2.4
Liver during PVP	130.5 ± 16.0	184.0 ± 32.0**	140.7 ± 20.6*	114.6 ± 13.8**	15.3 ± 4.2	129.1 ± 13.3	218.6 ± 52.5**	163.0 ± 35.3*	138.4 ± 25.1	19. 7 ± 6.1
Aorta during AP	300.9 ± 47.8	518.1 ± 66.1**	351.7 ± 43.6**	249.6 ± 29.9**	58.8 ± 8.1	319.7 ± 43.2	698.2 ± 170.5**	471.4 ± 111.9**	332.2 ± 76.2	80.2 ± 20.7
Portal vein during PVP	202.1 ± 29.3	349.5 ± 51.0**	249.7 ± 32.0**	173.1 ± 21.3**	38.4 ± 6.9	202.8 ± 22.3	446.7 ± 89.7**	305.6 ± 58.6**	218.4 ± 40.0*	49.8 ± 11.1
Muscle during AP	69.4 ± 12.8	53.5 ± 22.9**	51.2 ± 17.0**	49.6 ± 13.8**	2.2 ± 1.4	62.6 ± 12.3	65.4 ± 19.6	58.0 ± 15.0	52.7 ± 12.1*	2.6 ± 1.9
Muscle during PVP	78.1 ± 13.1	67.7 ± 25.0*	60.5 ± 17.9**	55.2 ± 14.5**	3.2 ± 2.0	70.1 ± 14.2	82.0 ± 17.7**	69.2 ± 12.4	60.7 ± 10.4*	3.5 ± 2.3
Image noise (HU)										
AP	12.8 ± 29.7	29.7 ± 15.0**	22.1 ± 11.6**	13.6 ± 9.3	–	11.2 ± 2.2	27.1 ± 6.9**	19.7 ± 5.0**	12.2 ± 3.4	–
PVP	15.7 ± 7.1	26.0 ± 4.9**	18.7 ± 3.6*	13.5 ± 2.7	–	13.5 ± 4.8	26.7 ± 4.8**	19.0 ± 3.5**	12.6 ± 3.3	–
CNR					CNR					
Liver during AP	1.6 ± 1.5	0.7 ± 0.7**	0.7 ± 0.9*	1.1 ± 1.1*	–	1.8 ± 1.7	0.7 ± 1.0**	0.8 ± 1.1*	1.1 ± 1.2*	–
Liver during PVP	3.7 ± 1.7	4.5 ± 1.4*	4.3 ± 1.4	4.8 ± 1.4	–	4.8 ± 2.0	5.3 ± 2.2	5.1 ± 2.0	4.9 ± 2.1	–
Aorta during AP	18.7 ± 8.8	18.3 ± 7.1	16.0 ± 6.4	15.4 ± 6.0	–	24.0 ± 6.6	24.8 ± 9.3	22.3 ± 8.4	21.0 ± 8.0	–
Portal vein during PVP	8.7 ± 3.2	11.0 ± 2.4**	9.7 ± 2.2	9.6 ± 2.7	–	10.6 ± 14.2	14.2 ± 4.4**	12.9 ± 4.1*	11.3 ± 3.6	–

Data are shown as the means ± standard deviation. The $p < 0.05$ indicates a statistically significant difference between protocol A and each energy level (keV) of protocol B or protocol C and each energy level (keV) of protocol D

IC iodine concentration, *ID* iodine (water)-based material decomposition images

*$p < 0.05$; **$p < 0.001$

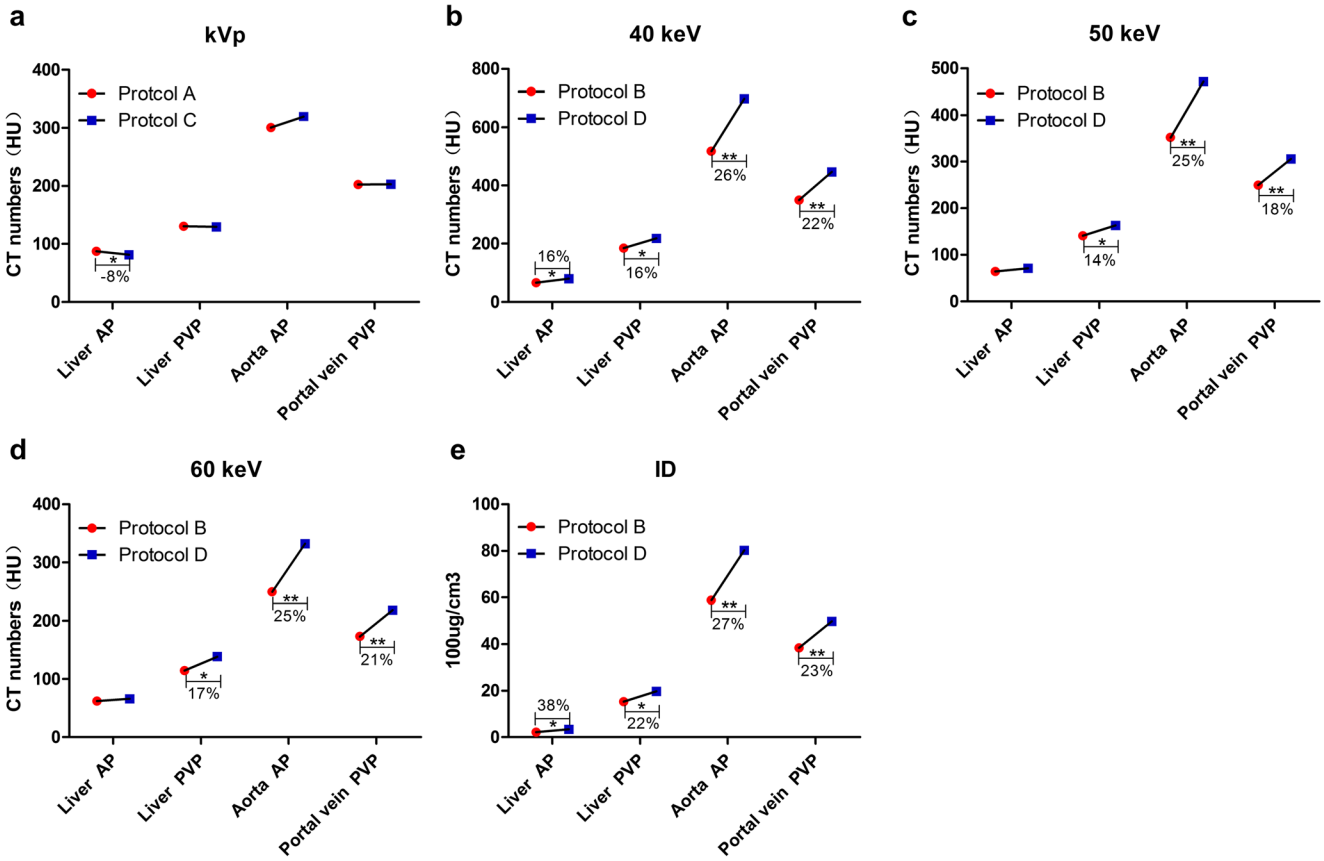

Fig. 4 Comparison of CT numbers in low-kVp CT images (**a**), VMIs with energy levels ranging from 40 to 60 keV (**b**, **c**, **d**), and iodine concentrations in iodine (water)-based material decomposition images (ID) (**e**) between images with 300 mg I/kg and those with 400 mg I/kg (*$p < 0.05$; **$p < 0.001$). The percentage increases in the values of organs were higher in VMIs and iodine-based images than in low-kVp CT images. Protocols A, B, C, and D used 80-kVp images, DECT images matched with 80-kVp images, 100-kVp images, and DECT images matched with 100 kVp, respectively. VMIs, virtual monochromatic images

quality appearance at low-keV images. These single-photon energy images, depicting objects with a theoretical monochromatic beam, can reduce beam-hardening artefacts and have higher attenuation than polychromatic CT images

Table 3 Qualitative analysis results in low-kVp protocols (protocols A and C) and spectral imaging protocols (protocols B and D)

Parameter	Protocol A	Protocol B			κ value	p value	Protocol C	Protocol D			κ value	p value
		40 keV	50 keV	60 keV				40 keV	50 keV	60 keV		
AP												
Small structures	3.9 ± 0.3	4.5 ± 0.1**	4.2 ± 0.1	3.4 ± 0.2*	0.732	< 0.001	3.7 ± 0.1	4.7 ± 0.1**	4.3 ± 0.1*	3.6 ± 0.2	0.722	< 0.001
Image noise	2.8 ± 0.6	2.6 ± 0.3*	3.0 ± 0.3	3.4 ± 0.4**	0.698	< 0.001	3.2 ± 0.3	2.8 ± 0.2*	3.2 ± 0.2	3.5 ± 0.3**	0.723	< 0.001
Overall quality	2.8 ± 0.2	2.6 ± 0.4	3.1 ± 0.4*	3.4 ± 0.3**	0.623	< 0.001	3.3 ± 0.2	2.8 ± 0.4*	3.2 ± 0.2	3.5 ± 0.4*	0.593	< 0.001
PVP												
Organ enhancement	2.4 ± 0.3	2.8 ± 0.1*	2.6 ± 0.1*	2.3 ± 0.2	0.728	< 0.001	2.4 ± 0.2	2.9 ± 0.1**	2.7 ± 0.2*	2.5 ± 0.2	0.707	< 0.001
Image noise	2.8 ± 0.2	2.6 ± 0.4*	3.0 ± 0.3	3.4 ± 0.2**	0.621	< 0.001	3.3 ± 0.2	2.8 ± 0.2**	3.1 ± 0.4	3.4 ± 0.2	0.663	< 0.001
Overall quality	2.7 ± 0.4	2.7 ± 0.2	3.3 ± 0.3*	3.4 ± 0.3**	0.669	< 0.001	3.2 ± 0.3	2.8 ± 0.1**	3.3 ± 0.4	3.5 ± 0.3*	0.662	< 0.001

Data are shown as the means ± standard deviation. A 3-point ordinal scale for organ enhancement and a 5-point scale for small structures, image noise, and overall quality were used; image quality increased as the grade increased (see the "Qualitative analysis" section). The $p < 0.05$ indicates a statistically significant difference between protocol A and each energy level (keV) of protocol B or protocol C and each energy level (keV) of protocol D. No cases were rated as unacceptable. κ value: the coefficient of inter-reader agreement

*$p < 0.05$; **$p < 0.001$

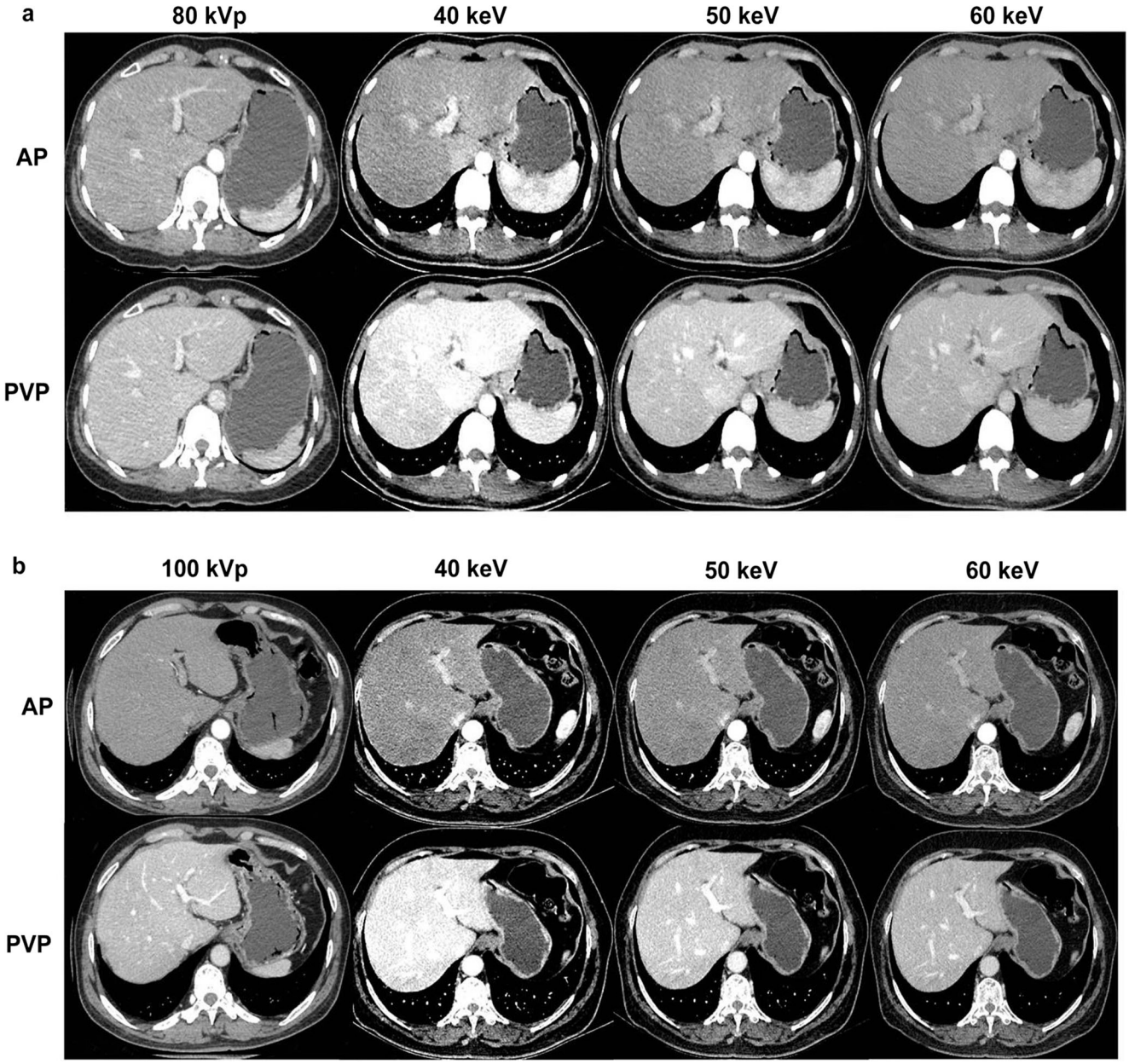

Fig. 5 Transverse contrast-enhanced low-kVp CT images (80 kVp, 300 mg I/kg, 46-year-old woman with a BMI of 20.28 kg/m^2; 100 kVp, 400 mg I/kg, 50-year-old man with a BMI of 24.44 kg/m^2) and corresponding DECT protocols with VMIs from 40 to 60 keV in a 28-year-old woman with a BMI of 21.28 kg/m^2 (**a**) and a 61-year-old woman with a BMI of 24.24 kg/m^2, respectively (**b**). The window setting was the same for all images, with a window width of 400 HU and window level of 40 HU. The overall image qualities for the images at 80 kVp were similar to those at 40 keV and lower than those at 50 keV and 60 keV. The overall image qualities for the images at 100 kVp were higher than those at 40 keV, similar to those at 50 keV, and lower than those at 60 keV. VMIs, virtual monochromatic images

[16, 34]. However, the CT number and CNR of VMIs in the liver during the AP, with low iodine intake, were lower than those in 80-kVp CT images in our study, which is similar to the results of Yu L et al [16]. In contrast to Yu L et al, who reported a lower iodine CNR in VMIs than in 80-kVp CT images, we observed a higher CNR in VMIs in organs with high iodine intake. This discrepancy may partially be explained by the fact that the results of Yu L et al were obtained with the same radiation dose used in the phantom, while our study was performed with the same noise index used in humans.

Of note, lower energy yields higher contrast by increasing the X-ray absorption of iodine. Compared to low-kVp images, 40- and 50-keV VMIs as well as iodine-based MD images may more closely approximate the k edge of iodine [32], leading to potentially greater confidence for the successful detection of lesions with similar or higher lesion conspicuity in our study, although this was not statistically significant for the

Table 4 Tumor-to-liver contrast ratio, lesion conspicuity, and detection rates of hepatocellular carcinomas in each protocol

Parameter	Protocol A ($n = 15$)	Protocol B ($n = 18$)				Protocol C ($n = 22$)	Protocol D ($n = 19$)			
		40 keV	50 keV	60 keV	ID		40 keV	50 keV	60 keV	ID
TNR[†]	1.55 ± 0.13	2.01 ± 0.17	1.62 ± 0.13	1.40 ± 0.09	2.03 ± 0.21	1.54 ± 0.18	2.26 ± 0.18	1.90 ± 0.22	1.65 ± 0.16	2.19 ± 0.25
p value	–	0.002	0.724	0.093	0.003	–	< 0.001	0.005	0.181	< .001
Lesion conspicuity[†]	3.38 ± 0.38	3.67 ± 0.12	3.35 ± 0.16	3.05 ± 0.16	3.67 ± 0.23	3.38 ± 0.08	3.75 ± 0.05	3.43 ± 0.10	3.12 ± 0.18	3.72 ± 0.31
p value	–	0.006	0.511	0.005	0.006	–	0.005	0.699	0.007	0.004
Detection rate[††]	100 (15/15)	100 (18/18)	94 (17/18)	83 (15/18)	100 (18/18)	100 (22/22)	100 (19/19)	100 (19/19)	89 (17/19)	100 (19/19)
p value	–	1	1	1	1	–	1	1	1	1

Numbers of lesions used to calculate the percentages are in brackets. The $p < 0.05$ indicates a statistically significant difference between protocol A and each energy level (keV) of protocol B or protocol C and each energy level (keV) of protocol D

TNR tumor-to-normal parenchyma ratio, *ID* iodine (water)-based material decomposition images

[†] Data are shown as the means ± standard deviation

[††] Data are percentages

tumor detection rate. Moreover, since the attenuation of low-kVp CT is sometimes affected by beam hardening and scanning parameters, the IC in MD image can be used as a more reliable measurement of tissue enhancement. The IC can directly quantify the iodinated contrast agent uptake and may serve as an independent surrogate marker of inherent tissue attenuation [32].

ASIS is designed to automatically generate the optimal spectral imaging presets to help achieve an accurate conventional scan mode CTDIvol value at the same noise index [13]. In our study, the radiation doses of the DECT and 100-kVp protocols were similar, which was consistent with the findings of a study by Wichmann JL et al [25]that compared the third-generation dual-source DECT and SECT with 100-kVp CT and verified the principle of the ASIS technique. A slight but significant increase (10%) in radiation dose was observed with DECT compared with that of 80-kVp CT, perhaps due to the higher effective voltage level (approximately 96 kVp) caused by the photon starvation of 80-kVp images, the failure of voltage-specific tube current modulation in DECT [35] and a milliampere increase in DECT without tube current modulation. Moreover, patients in the low-kVp and DECT groups were both susceptible to the low-kVp limitations of the scanner and patient, such as patient size, focal spot blurring, and tube current limitations. DECT with ASIS could not deliver the required low tube current, as observed with 80-kVp CT, due to the limited CTDIvol range available in the ASIS system, resulting in better image quality as well as a higher radiation dose.

Our study had several limitations. First, this study reflected our preliminary experience with a relatively small selected patient cohort. Second, the comparison of SECT and DECT was conducted in groups of patients with similar BMIs but not in the same patient cohort due to radiation concerns, which may have influenced the results of the study. Third, the CT protocol in this study was not dedicated to a specific clinical task but rather was focused on the general abdominal area. Fourth, the study was limited to extrapolation due to vendor-specific techniques with 50% ASIR. Lastly, iodine-suppressed virtual unenhanced images reconstructed with 70-keV VMIs were not investigated in our study, and this technique has shown the potential to replace true nonenhanced images and further reduce the radiation dose in DECT [36]. These results only apply to the scanner and implementation tested, but the findings might be useful as a reference when performing similar experiments in other types of scanners.

In conclusion, VMIs with an energy level at 50 keV in abdominal DECT provided overall image quality and lesion

Table 5 CTDIvol in low-kVp protocols (protocols A and C) and DECT protocols (protocols B and D) with the ASIS technique

CT parameter	Protocol A	Protocol B						Protocol C	Protocol D			
GSI preset	–	49	37	45	23	28	11	–	49	23	28	11
Number	$n = 60$	$n = 7$	$n = 4$	$n = 14$	$n = 29$	$n = 5$	$n = 1$	$n = 60$	$n = 1$	$n = 10$	$n = 18$	$n = 31$
CTDIvol (mGy)	7.07–8.47	6.94	7.86	8.07	11.32	17.89	19.11	10.96–18.97	6.94	11.32	17.89	19.11

GSI Gemstone Spectral Imaging, *ASIS* automatic spectral imaging selection

detectability that was similar to or higher than those of low-kVp images. The radiation dose in DECT with ASIS was slightly higher than that of 80-kVp CT, as it was increased by 10%, but it was similar to that of 100-kVp CT. Therefore, for patients with a BMI ≤ 23.9 kg/m^2 who have no desire to obtain material-specific information from DECT, an 80-kVp CT scan may be a better choice than a DECT scan.

Funding This study has received funding by National Natural Science Fund of China (Grant No. 81301220 to P. J. L.) and Overseas Research Project of Science and Technology Talent of Henan Health and Family Planning Commission (Grant No. 2018134 to P. J. L.)

Compliance with ethical standards

Guarantor The scientific guarantor of this publication is Jianbo Gao.

Conflict of interest The authors of this manuscript declare no relationships with any companies, whose products or services may be related to the subject matter of the article.

Statistics and biometry No complex statistical methods were necessary for this paper.

Informed consent Written informed consent was obtained from all subjects (patients) in this study.

Ethical approval Institutional Review Board approval was obtained.

Methodology
- prospective
- observational
- performed at one institution

References

1. Lee KH, Lee JM, Moon SK et al (2012) Attenuation-based automatic tube voltage selection and tube current modulation for dose reduction at contrast-enhanced liver CT. Radiology 265:437–447
2. Marin D, Nelson RC, Schindera ST et al (2010) Low-tube-voltage, high-tube-current multidetector abdominal CT: improved image quality and decreased radiation dose with adaptive statistical iterative reconstruction algorithm–initial clinical experience. Radiology 254:145–153
3. Marin D, Nelson RC, Samei E et al (2009) Hypervascular liver tumors: low tube voltage, high tube current multidetector CT during late hepatic arterial phase for detection–initial clinical experience. Radiology 251:771–779
4. Schindera ST, Diedrichsen L, Müller HC et al (2011) Iterative reconstruction algorithm for abdominal multidetector CT at different tube voltages: assessment of diagnostic accuracy, image quality, and radiation dose in a phantom study. Radiology 260:454–462
5. Marin D, Nelson RC, Barnhart H et al (2010) Detection of pancreatic tumors, image quality, and radiation dose during the pancreatic parenchymal phase: effect of a low-tube-voltage, high-tube-current CT technique–preliminary results. Radiology 256:450–459
6. Lv P, Lin XZ, Chen K, Gao J (2012) Spectral CT in patients with small HCC: investigation of image quality and diagnostic accuracy. Eur Radiol 22:2117–2124
7. Noda Y, Kanematsu M, Goshima S et al (2015) Reducing iodine load in hepatic CT for patients with chronic liver disease with a combination of low-tube-voltage and adaptive statistical iterative reconstruction. Eur J Radiol l84:11–18
8. Yamada Y, Jinzaki M, Hosokawa T, Tanami Y, Abe T, Kuribayashi S (2014) Abdominal CT: an intra-individual comparison between virtual monochromatic spectral and polychromatic 120-kVp images obtained during the same examination. Eur J Radiol 83:1715–1722
9. Marin D, Boll DT, Mileto A, Nelson RC (2014) State of the art: dual-energy CT of the abdomen. Radiology 271:327–342
10. Solomon J, Mileto A, Nelson RC, Roy Choudhury K, Samei E (2016) Quantitative features of liver lesions, lung nodules, and renal stones at multi-detector row CT examinations: dependency on radiation dose and reconstruction algorithm. Radiology 279:185–194
11. Lv P, Liu J, Yan X et al (2017) CT spectral imaging for monitoring the therapeutic efficacy of VEGF receptor kinase inhibitor AG-013736 in rabbit VX2 liver tumours. Eur Radiol 27:918–926
12. Marin D, Davis D, Roy Choudhury K et al (2017) Characterization of small focal renal lesions: diagnostic accuracy with single-phase contrast-enhanced dual-energy CT with material attenuation analysis compared with conventional attenuation measurements. Radiology 284:737–747
13. Lv P, Liu J, Chai Y, Yan X, Gao J, Dong J (2017) Automatic spectral imaging protocol selection and iterative reconstruction in abdominal CT with reduced contrast agent dose: initial experience. Eur Radiol 27:374–383
14. De Cecco CN, Darnell A, Macías N et al (2013) Second-generation dual-energy computed tomography of the abdomen: radiation dose comparison with 64- and 128-row single-energy acquisition. J Comput Assist Tomogr 37:543–546
15. Purysko AS, Primak AN, Baker ME et al (2014) Comparison of radiation dose and image quality from single-energy and dual-energy CT examinations in the same patients screened for hepatocellular carcinoma. Clin Radiol 69:e538–e544
16. Yu L, Christner JA, Leng S, Wang J, Fletcher JG, McCollough CH (2011) Virtual monochromatic imaging in dual-source dual-energy CT: radiation dose and image quality. Med Phys 38:6371–6379
17. Chen YA, Prabhudesai V, Castel H, Gupta S (2016) CT scan does not differentiate patients with hepatopulmonary syndrome from other patients with liver disease. PLoS One 11:e0158637
18. Yedibela S, Elad L, Wein A et al (2005) Neoadjuvant chemotherapy does not increase postoperative complication rate after resection of colorectal liver metastases. Eur J Surg Oncol 31:141–146
19. WHO Expert Consultation (2004) Appropriate body-mass index for Asian populations and its implications for policy and intervention strategies. Lancet 363:157–163
20. Ichikawa T, Erturk SM, Araki T (2006) Multiphasic contrast-enhanced multidetector-row CT of liver: contrast-enhancement theory and practical scan protocol with a combination of fixed injection duration and patients' body-weight-tailored dose of contrast material. Eur J Radiol 58:165–176
21. Gervaise A, Naulet P, Beuret F et al (2014) Low-dose CT with automatic tube current modulation, adaptive statistical iterative reconstruction, and low tube voltage for the diagnosis of renal colic: impact of body mass index. AJR Am J Roentgenol 202:553–560
22. Zhu Z, Zhao XM, Zhao YF, Wang XY, Zhou CW (2015) Feasibility study of using Gemstone Spectral Imaging (GSI) and adaptive statistical iterative reconstruction (ASIR) for reducing radiation and iodine contrast dose in abdominal CT patients with high BMI values. PLoS One 10:e0129201
23. Awai K, Takada K, Onishi H, Hori S (2002) Aortic and hepatic enhancement and tumor-to-liver contrast: analysis of the effect of different concentrations of contrast material at multi-detector row helical CT. Radiology 224:757–763

24. Lv P, Lin XZ, Li J, Li W, Chen K (2011) Differentiation of small hepatic hemangioma from small hepatocellular carcinoma: recently introduced spectral CT method. Radiology 259:720–729
25. Wichmann JL, Hardie AD, Schoepf UJ et al (2017) Single- and dual-energy CT of the abdomen: comparison of radiation dose and image quality of 2nd and 3rd generation dual-source CT. Eur Radiol 27(2):642–650
26. Nakayama Y, Awai K, Funama Y et al (2005) Abdominal CT with low tube voltage: preliminary observations about radiation dose, contrast enhancement, image quality, and noise. Radiology 237: 945–951
27. Christner JA, Kofler JM, McCollough CH (2010) Estimating effective dose for CT using dose-length product compared with using organ doses: consequences of adopting International Commission on Radiological Protection publication 103 or dual-energy scanning. AJR Am J Roentgenol 194:881–889
28. Roch P, Aubert B (2013) French diagnostic reference levels in diagnostic radiology, computed tomography and nuclear medicine: 2004-2008 review. Radiat Prot Dosimetry 154:52–75
29. Simantirakis G, Hourdakis CJ, Economides S et al (2015) Diagnostic reference levels and patient doses in computed tomography examinations in Greece. Radiat Prot Dosimetry 163:319–324
30. Treier R, Aroua A, Verdun FR, Samara E, Stuessi A, Trueb PR (2010) Patient doses in CT examinations in Switzerland: implementation of national diagnostic reference levels. Radiat Prot Dosimetry 142:244–254
31. Palorini F, Origgi D, Granata C, Matranga D, Salerno S (2014) Adult exposures from MDCT including multiphase studies: first Italian nationwide survey. Eur Radiol 24:469–483
32. Agrawal MD, Pinho DF, Kulkarni NM, Hahn PF, Guimaraes AR, Sahani DV (2014) Oncologic applications of dual-energy CT in the abdomen. Radiographics 34:589–612
33. Matsumoto K, Jinzaki M, Tanami Y, Ueno A, Yamada M, Kuribayashi S (2011) Virtual monochromatic spectral imaging with fast kilovoltage switching: improved image quality as compared with that obtained with conventional 120-kVp CT. Radiology 259:257–262
34. Yu L, Leng S, McCollough CH (2012) Dual-energy CT-based monochromatic imaging. AJR Am J Roentgenol 199:S9–S15
35. Simons D, Kachelriess M, Schlemmer HP (2014) Recent developments of dual-energy CT in oncology. Eur Radiol 24:930–939
36. Chai Y, Xing J, Gao J et al (2016) Feasibility of virtual nonenhanced images derived from single-source fast kVp-switching dual-energy CT in evaluating gastric tumors. Eur J Radiol 85:366–372